J Bionic Eng 17 (2020) 123–133
DOI: https://doi.org/10.1007/s42235-020-0010-y

Journal of Bionic Engineering
https://www.springer.com/journal/42235

Hydrodynamic Analysis and Verification of an Innovative Whale Shark-like Underwater Glider

Huijie Dong[1,2], Zhengxing Wu[1,2], Min Tan[1,2], Junzhi Yu[1,3*]

1. *State Key Laboratory of Management and Control for Complex Systems*, *Institute of Automation*, *Chinese Academy of Sciences*, *Beijing* 100190, *China*
2. *University of Chinese Academy of Sciences*, *Beijing* 100049, *China*
3. *State Key Laboratory for Turbulence and Complex Systems*, *Department of Mechanics and Engineering Science*, *BIC-ESAT*, *College of Engineering*, *Peking University*, *Beijing* 100871, *China*

Abstract

This paper presents an innovative design for a biomimetic whale shark-like underwater glider aiming at the combination of high maneuverability and long duration. As a hybrid of the underwater glider and the robotic fish, its pectoral fins and tail can serve as not only the external control surfaces for attitude regulation during gliding but also the propellers for agile fish-like swimming mode. To verify the gliding capability of the whale shark-like glider and prepare for future dynamic analysis, the hydrodynamic coefficients, including drag, lift, sliding force, and corresponding moments are estimated through computational fluid dynamics method. In addition, the hydrodynamic analyses of the proposed glider and an equivalent conventional glider during steady gliding motion are executed for comparison. Extended experiments are performed to verify the downward gliding performance. The results reveal that the whale shark-like glider has less drag as well as higher lift-to-drag ratio and a markable gliding capability in practice. It may offer important inspiration for improving the gliding efficiency and performance of an underwater glider in biomimetic shape design.

Keywords: biomimetic robot, CFD, hydrodynamic analysis, underwater glider

1 Introduction

As self-propelled unmanned underwater vehicles, underwater gliders are flourishingly developed and applied to explore the marine environment and make discoveries in these decades[1–3]. The underwater glider propels itself through adjusting net buoyancy and attitude instead of external active propulsion systems[4]. Through buoyancy adjustment system, movable internal mass, wings, and rudder, it can glide upwards or downwards in a sawtooth pattern at a relatively slow speed so that it has long-range and long-duration capabilities which enormously promotes the applications in huge oceans.

Conventional gliders are generally designed with a torpedo-like shape, a pair of wings for lift, and extra rudders for turning, such as Seaglider[5], Slocum[6], Spray[7], and Sea-Wing[8]. To reduce the drag, some gliders in biomimetic shapes have been presented[9–13]. Thereinto, the fish-like glider is appealing as the hybrid of underwater gliders and robotic fish. The robotic fish is more maneuverable by mimicking the shape and locomotive patterns of fish[14–16] so that by means of the integration of rudder with propeller, the fish-like gliders can possess both long-duration capability of the underwater glider and the maneuverability of the robotic fish. Zhang *et al*. presented a miniature fish-like underwater glider[10]. It is designed with a pair of large wings instead of the pectoral fins for enough lift and has no control surface as rudder or propeller. Zhou *et al*. presented a manta ray robot that can perform both flapping motion and gliding locomotion, but low space utilization is inevitable due to its shape[11]. Yuan *et al.* designed a gliding robotic dolphin as a hybrid of the underwater glider and the robotic dolphin[12], which is also developed for deep-sea application[13]. The gliding motion of the robotic dolphin relies on its horizontal flukes that can generate lift during gliding, but this way also brings the weak capability of yaw motion caused by the lack of an independent vertical control surface. Consequently, an innovative underwater glider needed to be developed to pursue both great gliding performance and high ma-

***Corresponding author:** Junzhi Yu
E-mail: junzhi.yu@ia.ac.cn

neuverability. In this paper, we offer a miniature bio-inspired underwater glider modeled after a whale shark with the consideration of its shape and natural habits.

The efficiency as well as the performance of an underwater glider mostly depends on the hydrodynamic characteristics such as lift, drag, and lift-to-drag ratio[17]. Computational Fluid Dynamics (CFD) simulation is an effective method to analyze hydrodynamic characteristics of an underwater glider[18–21]. Wu *et al*. designed a miniature dolphin-like glider and analyzed hydrodynamic performance in gliding motion by CFD method[18]. Wang *et al*. optimized the geometric model of the flying-wing structure underwater glider *via* CFD simulation aiming at the maximum lift-to-drag ratio[19]. Li *et al*. investigated the effect of aspect ratio in an underwater glider with a pair of flapping wings[20]. For gliding performance analysis, we also perform the CFD simulation for hydrodynamic modeling and analysis.

The main objective of this paper is to propose an innovative whale shark-like underwater glider and its hydrodynamic analysis. As a hybrid of the underwater glider and the robotic fish, it realizes an integration of rudder with propeller and a biomimetic shape like a whale shark. A miniature prototype is designed with a space-saving construct. Different from the conventional gliders, the proposed glider has a vertical tail and a pair of horizontal pectoral fins for both attitude adjustment and fish-like swimming. The hydrodynamic forces and moments of the body, the pectoral fins, and the tail are separately modeled *via* the CFD simulation for future dynamic analysis. In addition, the lift-to-drag ratio, surface pressure distribution, and flow velocity filed of both the proposed glider and an equivalent conventional glider are simulated and compared. The actual gliding performance is tested in experiments. The results show that the whale shark-like glider has a significantly large lift-to-drag ratio especially at a low Angle of Attack (AOA) and a remarkable gliding capability. This study contributes to research and development of the bioinspired underwater glider.

The remainder of this paper is organized as follows. Section **2** introduces the mechatronic design of the innovative whale shark-like glider. Section **3** details the hydrodynamic model of the proposed glider. The hydrodynamic characteristics and analysis are provided in section **4**. Extended experiments are performed in section **5**. Finally, section **6** gives concluding remarks and future work.

2 Whale shark-like glider design

The whale shark is the largest known fish, with the largest specimen recorded at 20 meters long. It has a broad, flattened head, a spindle shaped, fusiform body, and a semi-lunate caudal fin[21]. The migration study suggested that the whale shark is capable of long-distance travel[22]. Different from many bony fish who have a swim bladder that provides buoyancy and can help to keep the fish afloat, as a kind of cartilaginous fish, its streamlined shape keeps resistance to a minimum and it lifts itself by swimming instead of a swim bladder[23], which indicates its shape has an excellent locomotion capability. In this paper, an underwater glider is designed with a streamlined body shape by mimicking a whale shark. Fig. 1 shows the proposed whale shark-like glider with its mechanical structure.

The proposed glider is about 0.47 m long, 0.26 m wide, and weighs about 2.2 kg. A pair of pectoral fins and a tail are served as the external control surfaces to

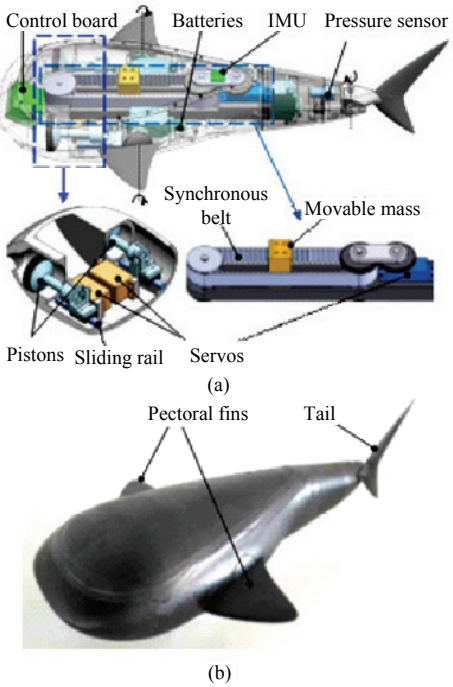

Fig. 1 Mechanical structure and prototype of the whale shark-like underwater glider. (a) Mechanical design; (b) robotic prototype.

regulate gliding motion or propel itself like a real fish. The tail can swing in the range of ±60°. The pectoral fins can pitch up or down in the range of ±90° actuated by two servos so that they can be deflected at the same or different angles as required. The shape of the fins is designed based on the real pectoral fins of a whale shark instead of large-aspect-ratio wings to improve the maneuverability. The internal actuators consist of a buoyancy adjustment system and a movable mass system whose structures are illustrated in Fig. 1. The buoyancy adjustment system is used to change the buoyancy for the driving force of gliding. Considering the special shape of the glider and to improve the space utilization, we design two piston units driven by two DC servos, respectively, which are controlled synchronously to maintain the same positions of the pistons. The buoyancy adjustment system can suck water up to 60 g within 0.5 s and yield the net buoyancy up to 0.294 N, about 1.36% of the whole displacement. Considering that the whale shark-like glider may not obtain enough pitch moments from the buoyancy adjustment system and the controllable pectoral fins, we design a conventional movable mass system. The system can shift a movable mass longitudinally for attitude regulation. The mass is about 0.2 kg and clings to the synchronous belt. A servo motor drives a synchronous pulley to make the mass move in a linear orbit in the range of ±4 cm so that the mass can rapidly reach the expected position. According to the experimental test, the pitch angle can be changed about ±40° in a state of equilibrium. The robot is also equipped with a wireless communication module and onboard sensors including an Inertial Measurement Unit (IMU) and a pressure sensor to separately measure real-time Euler angles, angular velocities, and diving depth. Table 1 lists the details of the employed components.

Table 1 Selected components used in the proposed glider

Component name	Component model
Controller	STM32F407
Piston servos	Kingmax BLS04L (3.6 Nm)
Fins servos	Hitec HS-7775MG (0.9 Nm)
Movable mass servo	Xunlongzhe DG-2020MG (3.2 Nm)
Communication module	RF200
IMU	MPU9250
Pressure sensor	MEAS MS5837-30BA

3 Hydrodynamic modelling

The gliding motion is the co-product of the net buoyancy and hydrodynamic forces. Thus, it is necessary to model the hydrodynamic force conditions for dynamical analysis of the gliding motion. The CFD simulation is an effective approach to acquire the hydrodynamic force conditions during gliding. Because of the controllable fins, the glider is divided into four parts, the body, the left pectoral fin, the right pectoral fin, and the tail, for hydrodynamic modelling with the quasi-steady lift resistance model method[24]. For an accurate and convenient CFD simulation, the commercial software SOLIDWORKS Flow Simulation is employed[25,26]. In simulation, unstructured mesh is formed, the velocity inlet with v = 0.3 m·s^{-1} and the pressure outlet are both three times body length away from the robot, the fluid is supposed as an incompressible and steady one, and k–ω Shear-Stress-Transport (SST) turbulence model with low-*Re* corrections is adopted. The computational domain and mesh generation are shown in Fig. 2. The linear velocity vector of the glider

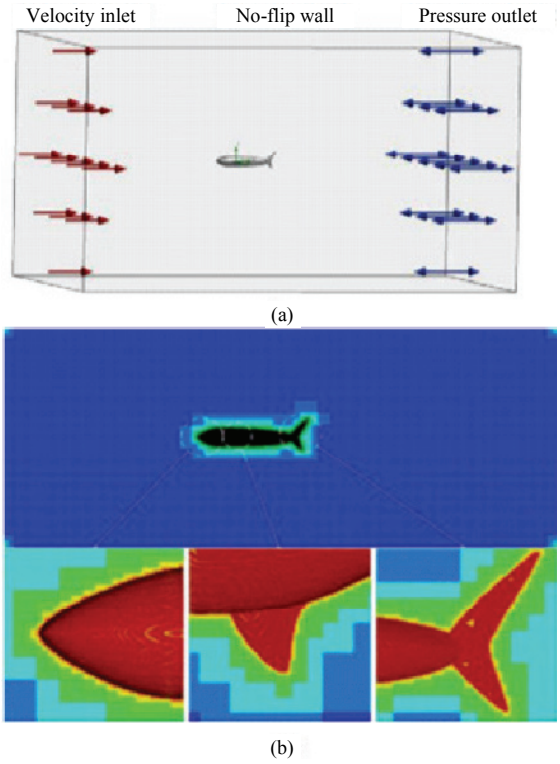

Fig. 2 Computational domain and mesh of the glider. (a) Computational domain and boundary conditions; (b) mesh generation.

is defined as $\boldsymbol{v_b} = (v_1, v_2, v_3)^{\mathrm{T}}$ and the angular velocity vector is defined as $\boldsymbol{w_b} = (w_1, w_2, w_3)^{\mathrm{T}}$. Hydrodynamic forces of each part are decomposed in the drag D, the slide force S, and the lift L. Corresponding moments are denoted as M_1, M_2, and M_3.

3.1 Body part

The hydrodynamic forces of the body are related with the AOA, α, and the sideslip angle, β, which are obtained by the velocity of the robot in the body frame as:

$$\alpha=\arctan(v_3 / v_1), \beta = \arcsin(v_2 / \|\boldsymbol{v_b}\|). \tag{1}$$

The hydrodynamic forces of the body can be expressed as:

$$\begin{cases} \boldsymbol{F}_b = \boldsymbol{R}_{bv}(-D_b, S_b, -L_b)^{\mathrm{T}} \\ \quad = \rho\|\boldsymbol{v}_b\|^2 \boldsymbol{R}_{bv}\left(C_{Db}(\alpha,\beta), C_{Sb}(\alpha,\beta), C_{Lb}(\alpha,\beta)\right)^{\mathrm{T}} \\ \boldsymbol{T}_b = \left(M_{1b}, M_{2b}, M_{3b}\right)^{\mathrm{T}} \\ \quad = \rho\|\boldsymbol{v}_b\|^2 \boldsymbol{R}_{bv}\left(C_{1b}(\alpha,\beta), C_{2b}(\alpha,\beta), C_{3b}(\alpha,\beta)\right)^{\mathrm{T}} \end{cases}, \tag{2}$$

where ρ is the fluid density ratio to the water (the density of water is 998 kg·m^{-3} in this paper), C_{Db}, C_{Sb}, and C_{Lb} represent drag, slide force, and lift coefficients, respectively, C_{1b}, C_{2b}, and C_{3b} are corresponding moment coefficients, and $\boldsymbol{R}_{bv}$ is the rotation matrix parameterized by α and β. In practice, α may vary from −90° to 90° when changing state of the gliding motion. Therefore, α and β are changed artificially both in the range of ±90° (the interval is set to 5°) and then the forces and moments are calculated by the software. Then the hydrodynamic variables are obtained by polynomial fitting. The simulation results and fitting curves are shown in Fig. 3. The degree of each fitting curve is minimal with a high goodness-of-fit. The drag coefficient is simply expressed by the sum of $C_{Db}(\alpha)$ and $C_{Db}(\beta)$, which is unsuitable for the cases of both large α and large β but adequate for the dynamic analysis. The polynomials are as:

$$\begin{cases} C_{Db}(\alpha,\beta) = -3.591\alpha^4 - 0.2033\alpha^3 + 13.54\alpha^2 \\ \qquad + 0.3862\alpha - 0.6339\beta^4 - 0.01\beta^3 \\ \qquad + 4.361\beta^2 + 0.02\beta + 0.4575 \\ C_{Sb}(\alpha,\beta) = 1.514\beta^3 + 4.356\beta \\ C_{Lb}(\alpha,\beta) = -4.072\alpha^9 + 0.7768\alpha^8 + 23.57\alpha^7 \\ \qquad - 3.628\alpha^6 - 44.22\alpha^5 + 4.821\alpha^4 \\ \qquad + 23.3\alpha^3 - 1.461\alpha^2 + 7.299\alpha \\ \qquad - 0.05687 \\ C_{1b}(\alpha,\beta) = 0 \\ C_{2b}(\alpha,\beta) = -0.5713\alpha^3 + 1.339\alpha \\ C_{3b}(\alpha,\beta) = -0.077\beta^5 + 0.421\beta^3 - 0.281\beta \end{cases}. \tag{3}$$

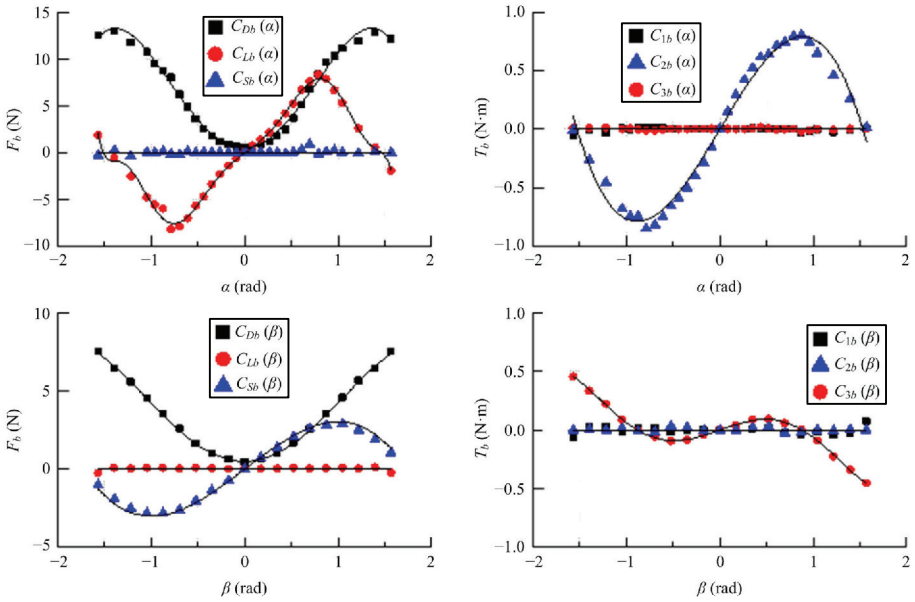

Fig. 3 Results and fitting curves of hydrodynamic variables of the body part.

3.2 Pectoral fins part

The linear velocity of the left pectoral fin centroid is denoted as:

$$\boldsymbol{v}_l = \boldsymbol{R}_{lb}(\boldsymbol{v}_b + \boldsymbol{w}_b \times \boldsymbol{P}_l)=(v_{l1}, v_{l2}, v_{l3})^{\mathrm{T}}, \tag{4}$$

where $\boldsymbol{P}_l = (p_{l1}, p_{l2}, p_{l3})^{\mathrm{T}}$ represents the position vector of the left pectoral fin and $\boldsymbol{R}_{lb}$ is the rotation matrix parameterized by the left pectoral fin's deflected angle δ_l. The AOA of the left pectoral fin is:

$$\alpha_l = \arctan(v_{l3} / v_{l1}). \tag{5}$$

The impact of sideslip is ignored because the fins can be approximate to slices. The hydrodynamic forces of the left pectoral fin contain the drag and the lift, therefore, the hydrodynamic forces on the body from the left pectoral fin can be expressed as:

$$\begin{cases} \boldsymbol{F}_l = \boldsymbol{R}_{lb}{}^{\mathrm{T}} \boldsymbol{R}_{lv} \left(-D_l, 0, -L_l\right)^{\mathrm{T}} \\ \quad = \rho \|\boldsymbol{v}_l\|^2 \boldsymbol{R}_{lb}{}^{\mathrm{T}} \boldsymbol{R}_{lv} \left(C_{Dl}(\alpha_l), 0, C_{Ll}(\alpha_l)\right)^{\mathrm{T}}, \\ \boldsymbol{T}_l = \left(M_{1l}, M_{2l}, M_{3l}\right)^{\mathrm{T}} = \boldsymbol{P}_l \times \boldsymbol{F}_l \end{cases} \tag{6}$$

where C_{Dl} and C_{Ll} are hydrodynamic variables, $\boldsymbol{R}_{lv}$ is the rotation matrix parameterized by α_l.

In the CFD simulation, α_l is changed artificially in the range of ±90° (the interval is set to 5°) and then the forces are calculated by the software. The simulation results and fitting curves are shown in Fig. 4. The polynomials are as:

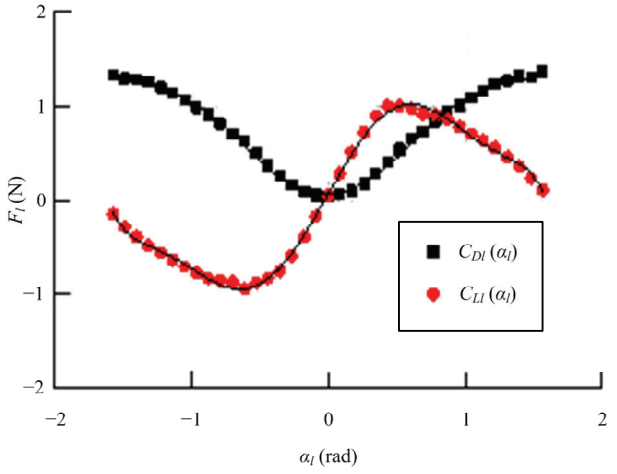

Fig. 4 Results and fitting curves of hydrodynamic variables of the left pectoral fin.

$$\begin{cases} C_{Dl}(\alpha_l) = 0.155\alpha_l^6 + 0.007\alpha_l^5 - 0.8586\alpha_l^4 \\ \qquad - 0.024\alpha_l^3 + 1.698\alpha_l^2 + 0.032\alpha_l \\ \qquad + 0.064 \\ C_{Ll}(\alpha_l) = -0.2817\alpha_l^7 - 0.0076\alpha_l^6 + 1.538\alpha_l^5 \\ \qquad + 0.0487\alpha_l^4 - 3.093\alpha_l^3 - 0.11\alpha_l^2 \\ \qquad + 2.563\alpha_l + 0.065 \end{cases}. \tag{7}$$

The two pectoral fins are symmetrical and of the same shape, so the hydrodynamic forces of the right pectoral fin can be obtained by conversion. The above all notations with subscript "*r*" are denoted the same as the notations with subscript "*l*".

$$\begin{cases} \boldsymbol{v}_r = \boldsymbol{R}_{rb}(\boldsymbol{v}_b + \boldsymbol{w}_b \times \boldsymbol{P}_r) = \left(v_{r1}, v_{r2}, v_{r3}\right)^{\mathrm{T}} \\ \alpha_r = \arctan\left(v_{r3} / v_{r1}\right) \\ \boldsymbol{F}_r = \boldsymbol{R}_{rb}{}^{\mathrm{T}} \boldsymbol{R}_{rv} \left(-D_r, 0, -L_r\right)^{\mathrm{T}} \\ \quad = \rho \|\boldsymbol{v}_r\|^2 \boldsymbol{R}_{rb}{}^{\mathrm{T}} \boldsymbol{R}_{rv} \left(C_{Dl}(\alpha_r), 0, C_{Ll}(\alpha_r)\right)^{\mathrm{T}} \\ \boldsymbol{T}_r = \left(M_{1r}, M_{2r}, M_{3r}\right)^{\mathrm{T}} = \boldsymbol{R}_{rb}{}^{\mathrm{T}} \boldsymbol{R}_{rv} \left(\boldsymbol{P}_r \times \boldsymbol{F}_r\right) \end{cases}. \tag{8}$$

3.3 Tail part

Similarly, the linear velocity of the tail is denoted as:

$$\boldsymbol{v}_t = \boldsymbol{R}_{tb}(\boldsymbol{v}_b + \boldsymbol{w}_b \times \boldsymbol{P}_t) = (v_{t1}, v_{t2}, v_{t3})^{\mathrm{T}}, \tag{9}$$

where $\boldsymbol{R}_{tb}$ is the rotation matrix parameterized by the tail's deflected angle δ_t. The sideslip angle of the tail is denoted as:

$$\beta_t = \arcsin\left(v_{t2} / \|\boldsymbol{v}_t\|\right). \tag{10}$$

The effect on hydrodynamic forces of the AOA of the tail is ignored. The hydrodynamic forces and moments on the robot generated by the tail are as:

$$\begin{cases} \boldsymbol{F}_t = \boldsymbol{R}_{tb}{}^{\mathrm{T}} \boldsymbol{R}_{tv} \left(-D_t, F_{st}, 0\right)^{\mathrm{T}} \\ \quad = \rho \|\boldsymbol{v}_t\|^2 \boldsymbol{R}_{tb}{}^{\mathrm{T}} \boldsymbol{R}_{tv} \left(C_{Dt}(\beta_t), C_{st}(\beta_t), 0\right)^{\mathrm{T}} \\ \boldsymbol{T}_t = \boldsymbol{R}_{tb}{}^{\mathrm{T}} \boldsymbol{R}_{tv} \left(M_{1t}, M_{2t}, M_{3t}\right)^{\mathrm{T}} \\ \quad = \boldsymbol{R}_{tb}{}^{\mathrm{T}} \boldsymbol{R}_{tv} \left(\boldsymbol{P}_t \times \boldsymbol{F}_t + \left(0, 0, C_{3t}(\beta_t)\right)^{\mathrm{T}}\right) \end{cases}. \tag{11}$$

The sideslip angle β_t is changed artificially in the range of ±90° (the interval is set to 5°) and then the forces are calculated by the software. The simulation results and fitting curves are shown in Fig. 5. The polynomials are as:

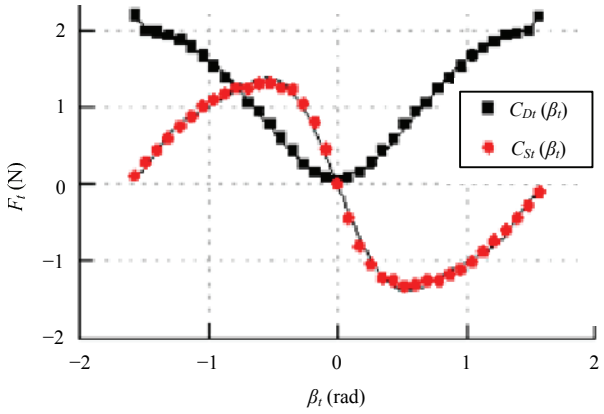

Fig. 5 Results and fitting curves of hydrodynamic variables of the tail.

$$\begin{cases} C_{Dt}(\beta_t) = 0.2672\beta_t^6 - 1.39\beta_t^4 + 2.643\beta_t^2 + 0.104 \\ C_{st}(\beta_t) = 0.4299\beta_t^9 - 2.762\beta_t^7 \\ \qquad + 6.515\beta_t^5 - 7.39\beta_t^3 + 4.218\beta_t \end{cases} . \quad (12)$$

3.4 Added mass calculation

When an underwater glider is in accelerated motion relative to surrounding fluid, it will be imposed an additional inertial force, which could be attributed to an equivalent added mass of fluid. The added mass is of fundamental importance in hydrodynamic research. It is hardly accurate to directly calculate the added mass of the whale shark-like glider by its complex shape. With the advancement in CFD methods, the added mass is calculated by simulating accelerated flows[27]. In the simulation, the initial fluid velocity is set to zero with an acceleration of 0.01 $m \cdot s^{-2}$. The force conditions of the glider in three directions are shown in Fig. 6.

As can be seen in Fig. 6, the forces are about 0.025 N, 0.034 N, and 0.050 N in the three directions. Based on the Newton's second law, the inertia mass of the glider is [2.5, 3.4, 5.0] kg. Subtracting mass of the glider, its added mass is [0.3, 1.2, 2.8] kg.

4 CFD analysis

For illustrating the hydrodynamic characteristics of the whale shark-like glider in detail, extended simulation is performed. A conventional underwater glider is also designed and the both lift-to-drag ratio, surface pressure, and velocity field is analyzed for comparison. The conventional glider is of the same length (except the tail), width, and displacement as the whale shark-like glider. The wings are designed with NACA 0016 aerofoil and also have the same position and chord as the pectoral fins. Its aspect ratio is about 1.32. Specific sizes are shown in Fig. 7.

4.1 Lift-to-drag ratio

The lift and drag of both gliders are calculated by CFD

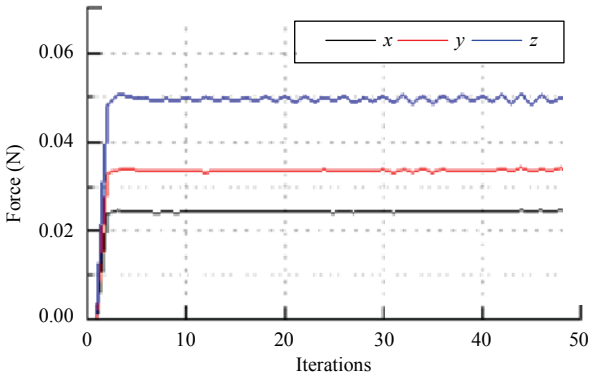

Fig. 6 Simulation results with the accelerated flows.

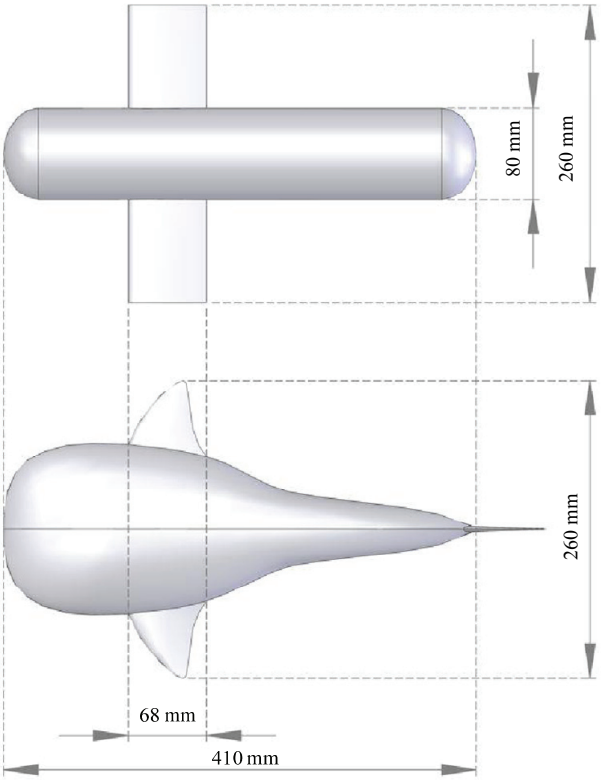

Fig. 7 Specific sizes of the conventional glider and the whale shark-like glider.

simulation with different AOA in range of 0° – 30°. The computational domain and boundary conditions are the same as section **3**. The results of their drag, lift, and lift-to-drag ratio are shown in Fig. 8. As can be seen, the whale shark-like glider has a remarkably smaller drag and higher lift-to-drag ratio, although the lift is a bit less than the conventional one. Especially at small AOA (lower than 10°), the lift of the proposed glider is similar with the conventional glider, meanwhile, the lift-to-drag ratio is significantly higher. These characteristics indicate the better performance of the proposed glider.

4.2 Surface pressure distribution

Figs. 9 and 10 separately show surface static pressure contour and values along the central line of lower surface for the both gliders at an AOA of 10° and an inlet velocity of 0.3 $m \cdot s^{-1}$. As can be seen, there is higher pressure at the heads of the gliders and the leading edges of wings (pectoral fins). It is noticed that the pressure of the proposed glider is more dispersive. It is observed in Fig. 10 that the static pressure is less and smoother in most part of the proposed glider.

4.3 Velocity field

Fig. 11 shows the flow velocity streamlines on the surface of the gliders at an AOA of 10° and an inlet velocity of 0.3 $m \cdot s^{-1}$ in detail. It is observed that the spatial distributions of velocity are not uniform. For the conventional glider, the flow velocity is low in head and rear. For the whale shark-like glider, however, the flow velocity is low in head but high in the front part, which illustrates that it has a higher lift-to-drag ratio although without wings of large aspect ratio.

5 Experiments

To verify the gliding performance of the proposed whale shark-like glider, extensive experiments have been performed. These experiments were conducted in an experimental pool (length: 5 m, width: 4 m, depth: 1.5 m) and were recorded by a camera installed on the side of the pool.

The gliding motion mainly depends on the net buoyancy and the attitude adjustment. In the experiments, we tested the downward gliding performance of the whale shark-like glider with different inputs including the displacement of the movable mass r_m and the net buoyancy m_0. The gliding motion was analyzed with the videos shot by the camera and the data collected by the onboard sensors. Figs. 12 and 13 illustrate the snapshot with gliding path and experimental results, respectively. The gliding path, the gliding angle, and the forward velocity were calculated *via* video processing. The AOA was calculated with the gliding angle and the pitch angle obtained by onboard IMU. The motion with the depth in range of 0.5 m – 1 m was regarded as the steady gliding motion to calculate the steady values.

As can be seen in Fig. 12, the whale shark-like glider successfully glided downwards to the bottom.

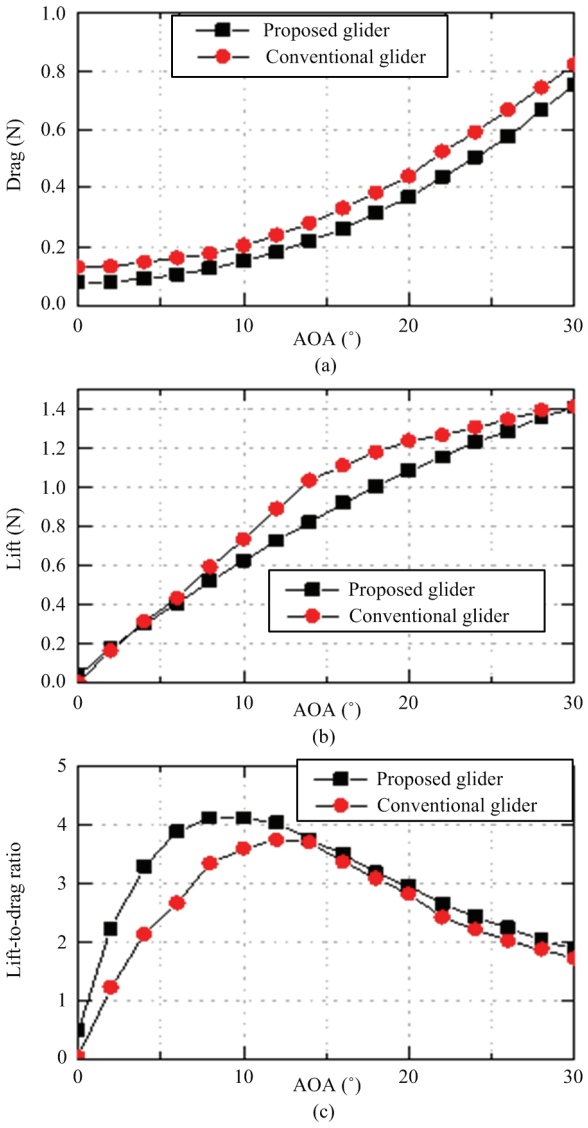

Fig. 8 Hydrodynamic forces and lift-to-drag ratio of the two gliders. (a) Drag values at different AOAs; (b) lift values at different AOAs; (c) lift-to-drag ratio values at different AOAs.

The gliding paths vary with different net buoyancies and different movable mass displacements. Obviously when $m_0 = -30$ g, the glider can move farther at the same depth. According to the experimental results, we can see that the whale shark-like glider could obtain the highest horizontal speed of about 0.24 m·s^{-1} when $r_m = -0.2$ m. The minimal gliding angle is about 28° at $r_m = -0.15$ m and $m_0 = -30$ g. The AOAs are all less than 10°, which are exactly in the range of higher lift-to-drag ratio in Fig. 8. Table 2 tabulates some metrics of existing underwater gliders and the proposed one. The achieved horizontal velocity per unit body length by our glider is much bigger than those of reported gliders. These results testify that the proposed whale shark-like glider has an excellent capability for gliding.

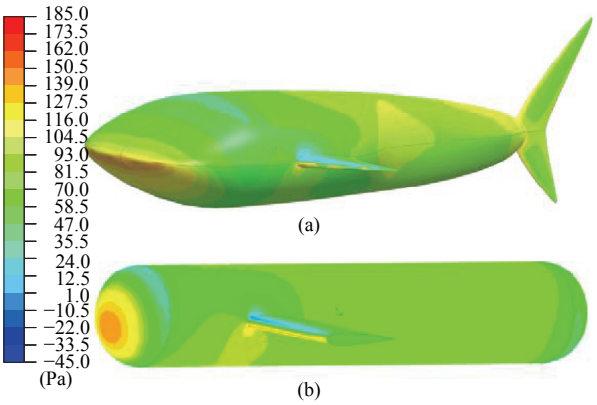

Fig. 9 Static pressure distribution at an AOA of 10° and an inlet velocity of 0.3 m·s^{-1}. (a) Whale shark-like glider; (b) conventional glider.

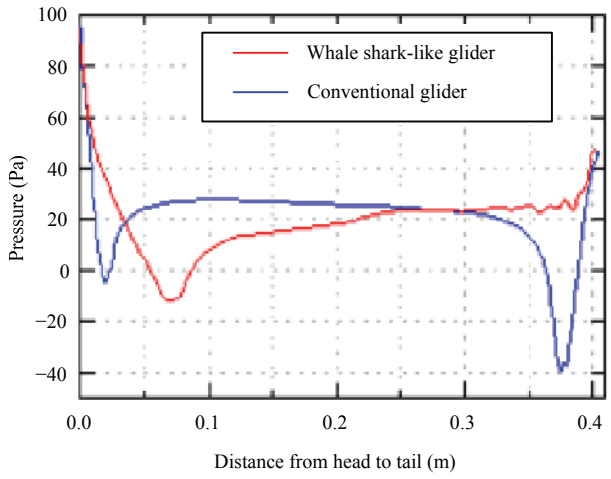

Fig. 10 Static pressure along the central line of lower surface.

Table 2 Metrics of different underwater gliders reported in the literatures

Name	Length (m)	Weight (kg)	Net buoyancy (g)	Velocity (m·s^{-1})	Velocity (body length per second)
Seaglider[5]	1.8	52	840	0.45	0.25
Slocum[6]	1.8	52	520	0.40	0.22
Spray[7]	2.0	51	900	0.45	0.23
Sea-Wing[8]	2.0	65	–	0.25	0.13
Miniature glider[28]	0.4	4	20	0.14	0.35
Petrel II[29]	1.8	70	–	0.65	0.36
Proposed glider	0.47	2.2	30	0.24	0.51

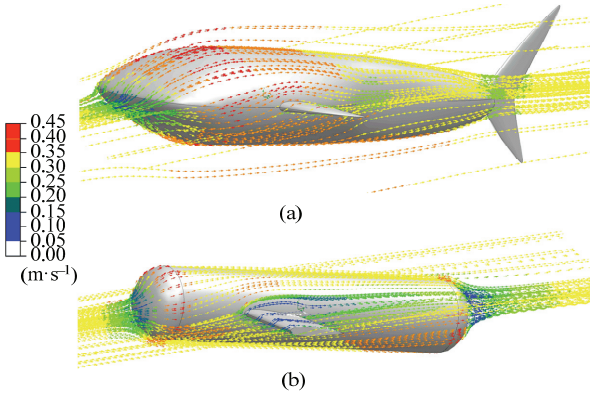

Fig. 11 Velocity stream lines at an AOA of 10° and an inlet velocity of 0.3 m·s^{-1}. (a) Whale shark-like glider; (b) conventional glider.

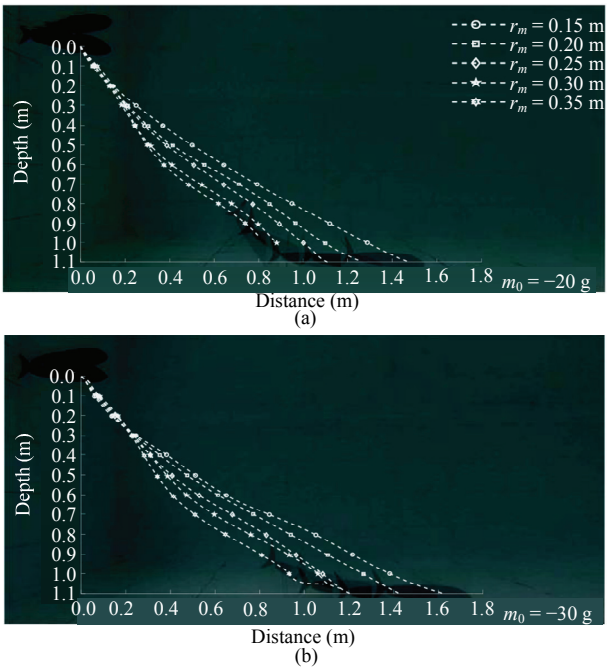

Fig. 12 Snapshot and gliding path of the experiments with different r_m. (a) Net buoyancy of −20 g; (b) net buoyancy of −30 g.

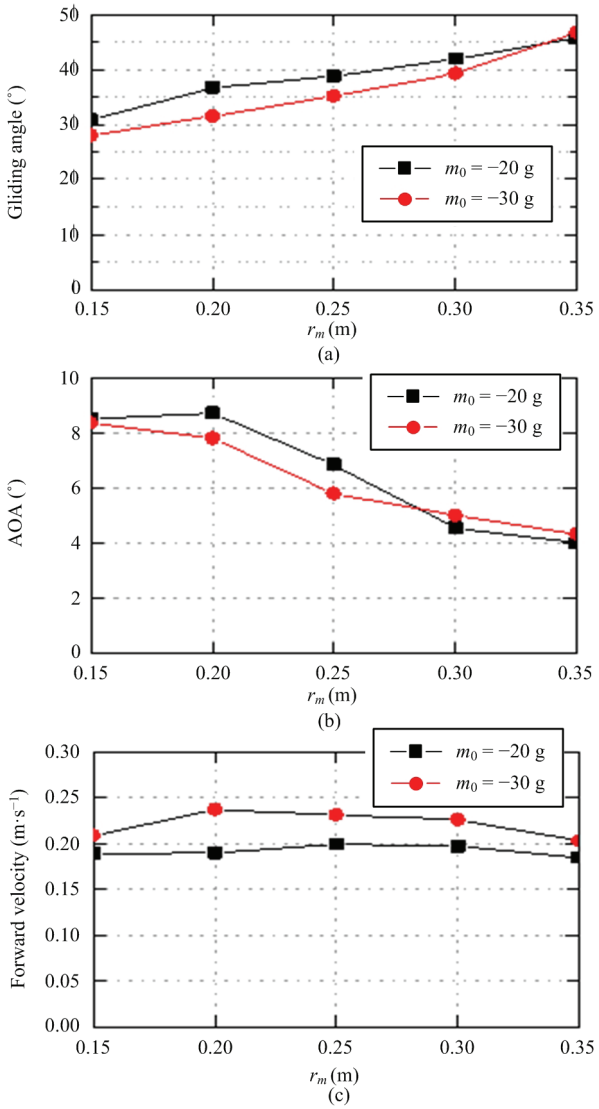

Fig. 13 Experimental results of the steady downward gliding motion with different inputs. (a) Steady gliding angle; (b) steady AOA; (c) steady forward velocity.

Although inevitable error exists, the CFD simulation is a convenient and efficient approach to test the hydrodynamic characteristics before prototyping. The experimental results verify the gliding performance of the whale shark-like glider indicated by the hydrodynamic analysis based on the CFD simulation. The obtained hydrodynamic coefficients should be corrected by future dynamic simulation and experiments.

Compared with the conventional one, the gliding attitude of the proposed glider can be regulated by the movable mass, the net buoyancy, and the fins. For better gliding performance, the net buoyancy can be set to extreme so that the movable mass and the fins can be the inputs for attitude control. Although the pectoral fins also can serve as horizontal control surface for pitch adjustment, we found that the effect on gliding motion of the small-angle deflection of the pectoral fins (±20°) is in apparent. This may be caused by the short force arm of the pectoral fins, flow disturbance, and the yaw error. Therefore, a dynamic model including the movable fins should be constructed for motion analysis.

6 Conclusion

In this paper, we have provided a novel whale shark-like underwater glider as well as its hydrodynamic analysis and verification. As a hybrid of the underwater glider and the robotic fish, it realizes an integration of rudder with propeller and a biomimetic shape like a whale shark. First, a miniature prototype is designed with a space-saving construct. The internal actuating system contains a movable mass and a pair of piston units for attitude and net buoyancy adjustment, respectively. The external control surfaces consist of a vertical tail and a pair of horizontal pectoral fins. Second, the hydrodynamic forces and moments of the body, the pectoral fins, and the tail are separately modeled via the CFD simulation for future dynamic analysis. Third, in order to analyze the gliding performance, a CAD model of an equivalent conventional glider with the same length, width, and displacement as the proposed glider is prepared, then the lift-to-drag ratio, surface pressure distribution, and flow velocity filed of the both gliders are simulated and compared. The results show that the whale shark-like glider has a significantly large lift-to-drag ratio especially at low AOA, indicating better gliding efficiency and performance. Finally, the downward gliding performance is verified by the experiments with different displacements of the movable mass and different net buoyancies. The obtained results contribute to innovative research and development of bioinspired underwater glider. Our ongoing and future work will focus on the motion analysis and intelligent control of the proposed underwater robot including the gliding motion and the fish-like swimming.

Acknowledgment

This work was supported by the National Natural

Science Foundation of China (Nos. 61725305, U1909206, 61421004, 61633017), the Pre-Research Fund of Equipment of China (No. 61402070304), the Beijing Natural Science Foundation (No. 4192060), and the Youth Innovation Promotion Association CAS (No. 2019138).

References

[1] Rudnick D L, Davis R E, Eriksen C C, Fratantoni D M, Perry M J. Underwater gliders for ocean research. *Marine Technology Society Journal*, 2004, **38**, 48–59.

[2] Zaba K D, Rudnick D L. The 2014–2015 warming anomaly in the Southern California current system observed by underwater gliders. *Geophysical Research Letters*, 2016, **43**, 1241–1248.

[3] Houpert L, Inall M E, Dumont E, Gary S, Johnson C, Porter M, Johns W E, Cunningham S A. Structure and transport of the north atlantic current in the eastern subpolar gyre from sustained glider observations. *Journal of Geophysical Research*: *Oceans*, 2018, **123**, 6019–6038.

[4] Shi Y, Shen C, Fang H, Li H. Advanced control in marine mechatronic systems: A survey. *IEEE*/*ASME Transactions on Mechatronics*, 2017, **22**, 1121–1131.

[5] Eriksen C C, Osse T J, Light R D, Wen T, Lehman T W, Sabin P L, Ballard J W, Chiodi A M. Seaglider: A long-range autonomous underwater vehicle for oceanographic research. *IEEE Journal of Oceanic Engineering*, 2001, **26**, 424–436.

[6] Webb D C, Simonetti P J, Jones C P. SLOCUM: An underwater glider propelled by environmental energy. *IEEE Journal of Oceanic Engineering*, 2001, **26**, 447–452.

[7] Sherman J, Davis R E, Owens W, Valdes J. The autonomous underwater glider "Spray". *IEEE Journal of Oceanic Engineering*, 2001, **26**, 437–446.

[8] Yu J C, Zhang F M, Zhang A Q, Jin W M, Tian Y. Motion parameter optimization and sensor scheduling for the sea-wing underwater glider. *IEEE Journal of Oceanic Engineering*, 2013, **38**, 243–254.

[9] Zhao L, Wang P, Sun C Y, Song B W. Modeling and motion simulation for a flying-wing underwater glider with a symmetrical airfoil. *China Ocean Engineering*, 2019, **33**, 322–332.

[10] Zhang F T, Thon J, Thon C, Tan X B. Miniature underwater glider: Design and experimental results. *IEEE*/*ASME Transactions on Mechatronics*, 2014, **19**, 394–399.

[11] Zhou C L, Low K H. Better endurance and load capacity: An improved design of manta ray robot (RoMan-II). *Journal of Bionic Engineering*, 2010, **7**, S137–S144.

[12] Yuan J, Wu Z X, Yu J Z, Zhou C, Tan M. Design and 3D motion modeling of a 300-m gliding robotic dolphin. *IFAC-Papers OnLine*, 2017, **50**, 685–690.

[13] Wu Z X, Yu J Z, Yuan J, Tan M. Towards a gliding robotic dolphin: Design, modeling, and experiments. *IEEE*/*ASME Transactions on Mechatronics*, 2019, **24**, 260–270.

[14] Wang Y W, Tan J B, Zhao D B. Design and experiment on a biomimetic robotic fish inspired by freshwater stingray. *Journal of Bionic Engineering*, 2015, **12**, 204–216.

[15] Xu D, Zeng H N, Peng X, Zhao Z Q, Liu J M. A stiffness adjustment mechanism based on negative work for high-efficient propulsion of robotic fish. *Journal of Bionic Engineering*, 2018, **15**, 270–282.

[16] Li K K, Jiang H Z, Wang S Y, Yu J M. A soft robotic fish with variable-stiffness decoupled mechanisms. *Journal of Bionic Engineering*, 2018, **15**, 599–609.

[17] Meyers L M. *Analysis of Lift and Drag Forces on the Wing of the Underwater Glider*. PhD Thesis, Cape Peninsula University of Technology, Cape Town, South Africa, 2018.

[18] Wu Z X, Yu J Z, Yuan J, Tan M. Analysis and verification of a miniature dolphin-like underwater glider. *Industrial Robot*, 2016, **43**, 628–635.

[19] Wang Z Y, Yu J C, Zhang A Q, Wang Y X, Zhao W T. Parametric geometric model and hydrodynamic shape optimization of a flying-wing structure underwater glider. *Chinese Ocean Engineering*, 2017, **31**, 709–715.

[20] Li Y C, Pan D Y, Ma Z, Zhao Q S. Aspect ratio effect of a pair of flapping wings on the propulsion of a bionic autonomous underwater glider. *Journal of Bionic Engineering*, 2019, **16**, 145–153.

[21] Rowat D, Brooks K S. A review of the biology, fisheries and conservation of the whale shark *Rhincodon typus*. *Journal of Fish Biology*, 2012, **80**, 1019–1056.

[22] Guzman H M, Gomez C G, Hearn A, Eckert S A. Longest recorded trans-pacific migration of a whale shark (*rhincodontypus*). *Marine Biodiversity Records*, 2018, **11**, 8.

[23] Hagler G. *Modeling Ships and Space Craft*. Springer, Berlin, Germany, 2013, 45–61.

[24] Nabawy M R A, Crowther W J. On the quasi-steady aerodynamics of normal hovering flight part II: Model implementation and evaluation. *Journal of the Royal Society Interface*, 2014, **11**, 20131197.

[25] Bellos E, Korres D, Tzivanidis C, Antonopoulos K A. Design, simulation and optimization of a compound parabolic collector. *Sustainable Energy Technologies and Assessments*, 2016, **16**, 53–63.

[26] Nedelcu D, Ianici D, Nedeloni M D, Daia D, Pop F M,

Avasiloaie R C. The hydrodynamic characteristics calculus for isolated profile Go428 using Solidworks flow simulation module. *Proceedings of the* 4*th WSEAS International Conference*, Paris, France, 2011, 92–97.

[27] Jie L, Lu C J, Huang X. Calculation of added mass of a vehicle running with cavity. *Journal of Hydrodynamics*, *Ser. B*, 2010, **22**, 312–318.

[28] Zhang F, Thon J, Thon C, Tan X. Miniature underwater glider: Design, modeling, and experimental results. *Proceedings of IEEE International Conference on Robotics and Automation*, Saint Paul, USA, 2012, 4904–4910.

[29] Liu F, Wang Y, Wang S. Development of the hybrid underwater glider PetreI-II. *Sea Technology*, 2014, **55**, 51–54.